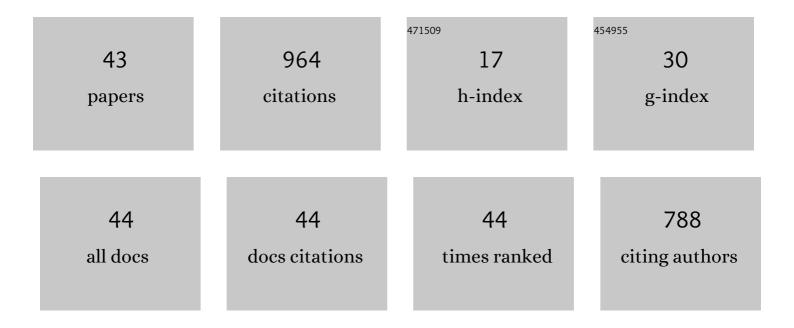
C S Carrano

List of Publications by Year in descending order

Source: https://exaly.com/author-pdf/7811498/publications.pdf Version: 2024-02-01



CSCAPPANO

#	Article	IF	CITATIONS
1	Performance of 6 Different Global Navigation Satellite System Receivers at Low Latitude Under Moderate and Strong Scintillation. Earth and Space Science, 2021, 8, e2020EA001314.	2.6	14
2	GNSS signal phase, TEC, and phase unwrapping errors. Navigation, Journal of the Institute of Navigation, 2020, 67, 865-873.	2.8	1
3	A twoâ€parameter multifrequency GPS signal simulator for strong equatorial ionospheric scintillation: modeling and parameter characterization. Navigation, Journal of the Institute of Navigation, 2020, 67, 181-195.	2.8	6
4	Wave Field Propagation in Extended Highly Anisotropic Media. Radio Science, 2019, 54, 646.	1.6	4
5	Effect of Anisotropy on Ionospheric Scintillations Observed by SAR. IEEE Transactions on Geoscience and Remote Sensing, 2019, 57, 6888-6899.	6.3	3
6	On the Relationship Between the Rate of Change of Total Electron Content Index (ROTI), Irregularity Strength (<i>C</i> _{<i>k</i>} <i>L</i>), and the Scintillation Index (<i>S</i> _{<i>4</i>}). Journal of Geophysical Research: Space Physics, 2019, 124, 2099-2112.	2.4	56
7	Stochastic TEC Structure Characterization. Journal of Geophysical Research: Space Physics, 2019, 124, 10571-10579.	2.4	12
8	Global Ionospheric Models, TEC, and Stochastic Structure. , 2019, , .		0
9	A Multifrequency GPS Signal Strong Equatorial Ionospheric Scintillation Simulator: Algorithm, Performance, and Characterization. IEEE Transactions on Aerospace and Electronic Systems, 2018, 54, 1947-1965.	4.7	17
10	Dynamic spectral characteristics of high-resolution simulated equatorial plasma bubbles. Progress in Earth and Planetary Science, 2018, 5, .	3.0	11
11	A Configuration Space Model for Intermediateâ€5cale Ionospheric Structure. Radio Science, 2018, 53, 1472-1480.	1.6	6
12	A compact multiâ€frequency GNSS scintillation model. Navigation, Journal of the Institute of Navigation, 2018, 65, 563-569.	2.8	19
13	Effect of Anisotropy on Ionospheric Scintillations Observed by Synthetic Aperture Radar (Sar). , 2018, ,		0
14	Ionospheric Scintillation Observation Using Spaceâ€Borne Synthetic Aperture Radar Data. Radio Science, 2018, 53, 1187-1202.	1.6	13
15	On the Characterization of Intermediateâ€Scale Ionospheric Structure. Radio Science, 2018, 53, 1316-1327.	1.6	5
16	Midlatitude Ionospheric Irregularity Spectral Density as Determined by Groundâ€Based GPS Receiver Networks. Journal of Geophysical Research: Space Physics, 2018, 123, 5055-5067.	2.4	10
17	HF propagation results from the Metal Oxide Space Cloud (MOSC) experiment. Radio Science, 2017, 52, 710-722.	1.6	9
18	A technique for inferring zonal irregularity drift from singleâ€station GNSS measurements of intensity (<i>S</i> ₄) and phase (<i>İf</i> _{Ìt}) scintillations. Radio Science, 2016, 51, 1263-1277.	1.6	17

C S CARRANO

#	Article	IF	CITATIONS
19	A theory of scintillation for twoâ€component power law irregularity spectra: Overview and numerical results. Radio Science, 2016, 51, 789-813.	1.6	46
20	A characterization of intermediateâ€scale spread <i>F</i> structure from fourÂyears of highâ€resolution C/NOFS satellite data. Radio Science, 2016, 51, 779-788.	1.6	19
21	The Influence of Equatorial Scintillation on L-Band SAR Image Quality and Phase. IEEE Transactions on Geoscience and Remote Sensing, 2016, 54, 869-880.	6.3	61
22	Ionospheric acoustic and gravity waves associated with midlatitude thunderstorms. Journal of Geophysical Research: Space Physics, 2015, 120, 6010-6020.	2.4	56
23	Digital signal processing for ionospheric propagation diagnostics. Radio Science, 2015, 50, 837-851.	1.6	2
24	Wavelet-based analysis and power law classification of C/NOFS high-resolution electron density data. Radio Science, 2014, 49, 680-688.	1.6	9
25	Characterization of GNSS scintillations over Lagos, Nigeria during the minimum and ascending phases (2009–2011) of solar cycle 24. Advances in Space Research, 2014, 53, 37-47.	2.6	26
26	Variation in total electron content above large thunderstorms. Geophysical Research Letters, 2013, 40, 1945-1949.	4.0	42
27	Comparison of equatorial GPS-TEC observations over an African station and an American station during the minimum and ascending phases of solar cycle 24. Annales Geophysicae, 2013, 31, 2085-2096.	1.6	58
28	Latitudinal and Local Time Variation of Ionospheric Turbulence Parameters during the Conjugate Point Equatorial Experiment in Brazil. International Journal of Geophysics, 2012, 2012, 1-16.	1.1	30
29	Equatorial plasma bubbles and L-band scintillations in Africa during solar minimum. Annales Geophysicae, 2012, 30, 675-682.	1.6	75
30	Simulating the impacts of ionospheric scintillation on L band SAR image formation. Radio Science, 2012, 47, .	1.6	77
31	The effect of phase scintillations on the accuracy of phase screen simulation using deterministic screens derived from GPS and ALTAIR measurements. Radio Science, 2012, 47, .	1.6	9
32	The application of numerical simulations in Beacon scintillation analysis and modeling. Radio Science, 2011, 46, .	1.6	9
33	Multiple phase screen modeling of ionospheric scintillation along radio occultation raypaths. Radio Science, 2011, 46, .	1.6	43
34	Equatorial scintillation characteristics during solar minimum: Observations from the SCINDA network. , 2011, , .		0
35	A phase screen simulator for predicting the impact of small-scale ionospheric structure on SAR image formation and interferometry. , 2010, , .		9
36	Specification of the occurrence of equatorial ionospheric scintillations during the main phase of large magnetic storms within solar cycle 23. Radio Science, 2010, 45, n/a-n/a.	1.6	46

C S CARRANO

#	Article	IF	CITATIONS
37	Total electron content processing from GPS observations to facilitate ionospheric modeling. GPS Solutions, 2009, 13, 83-95.	4.3	22
38	Kalman filter-based algorithms for monitoring the ionosphere and plasmasphere with GPS in near-real time. Journal of Atmospheric and Solar-Terrestrial Physics, 2009, 71, 158-174.	1.6	21
39	Simulating the effects of scintillation on transionospheric signals with a twoâ€way phase screen constructed from ALTAIR phaseâ€derived TEC. Radio Science, 2009, 44, .	1.6	12
40	Kalman filter estimation of plasmaspheric total electron content using GPS. Radio Science, 2009, 44, .	1.6	28
41	Impacts of the December 2006 solar radio bursts on the performance of GPS. Radio Science, 2009, 44, .	1.6	53
42	Detection of Ionospheric Structures with L-Band Synthetic Aperture Radars. , 2008, , .		3
43	A Fourier analysis and dynamic optimization of the Petrov-Galerkin finite element method. International Journal for Numerical Methods in Engineering, 1995, 38, 4123-4155.	2.8	5